Deep-space and near-Earth optical communications by coded orbital angular momentum (OAM) modulation

Ivan B. Djordjevic

University of Arizona, Depart. Electrical & Computer Eng., 1230 E. Speedway Blvd., Tucson, AZ 85721, USA
ivan@ece.arizona.edu

Abstract: In order to achieve multi-gigabit transmission (projected for 2020) for the use in interplanetary communications, the usage of large number of time slots in pulse-position modulation (PPM), typically used in deep-space applications, is needed, which imposes stringent requirements on system design and implementation. As an alternative satisfying high-bandwidth demands of future interplanetary communications, while keeping the system cost and power consumption reasonably low, in this paper, we describe the use of orbital angular momentum (OAM) as an additional degree of freedom. The OAM is associated with azimuthal phase of the complex electric field. Because OAM eigenstates are orthogonal the can be used as basis functions for *N*-dimensional signaling. The OAM modulation and multiplexing can, therefore, be used, in combination with other degrees of freedom, to solve the high-bandwidth requirements of future deep-space and near-Earth optical communications. The main challenge for OAM deep-space communication represents the link between a spacecraft probe and the Earth station because in the presence of atmospheric turbulence the orthogonality between OAM states is no longer preserved. We will show that in combination with LDPC codes, the OAM-based modulation schemes can operate even under strong atmospheric turbulence regime. In addition, the spectral efficiency of proposed scheme is $N^2/\log_2 N$ times better than that of PPM.

OCIS codes: (060.2605) Free-space optical communication; (060.4080) Modulation; (010.1330) Atmospheric turbulence; (1880) Detection; (120.6085) Space instrumentation

References and links

1. B. Moision and J. Hamkins, "Deep-space optical communications downlink budget: modulation and coding," The Interplanetary Network Progress Report 42-154, April-June 2003 (Jet Propulsion Laboratory, Pasadena, California, 15 August 2003), pp. 1-28, http://ipnpr.jpl.nasa.gov/progress_report/42-154/154K.pdf.
2. B. Moision and J. Hamkins, "Coded modulation for the deep-space optical channel: serially concatenated pulse-position modulation," The Interplanetary Network Progress Report 42-161 (Jet Propulsion Laboratory, Pasadena, California, 15 May 2005), pp. 1-25, http://ipnpr.jpl.nasa.gov/progress_report/42-161/161T.pdf.
3. F. Xu, M.-A. Khalighi, and S. Bourennane, "Coded PPM and multipulse PPM and iterative detection for free-space optical links," J. Opt. Commun. Netw. **1**(5), 404–415 (2009).
4. S. J. Dolinar, J. Hamkins, B. E. Moision, and V. A. Vilnrotter, "Optical modulation and coding," in *Deep Space Optical Communications*, H. Hemmati, ed. (Wile, 2006), pp. 215–299.
5. H. Hemmati, "Interplanetary laser communications," Optics & Photonics News **18**(11), 22–27 (2007).
6. L. C. Andrews and R. L. Philips, *Laser Beam Propagation through Random Media* (SPIE Press, 2005).
7. I. B. Djordjevic and M. Arabaci, "LDPC-coded orbital angular momentum (OAM) modulation for free-space optical communication," Opt. Express **18**(24), 24722–24728 (2010).
8. I. B. Djordjevic, "Orbital angular momentum (OAM) based LDPC-coded deep-space optical communication," Proc. SPIE **7923**, 792306, 792306–792308 (2011) (invited paper).
9. C. Paterson, "Atmospheric turbulence and orbital angular momentum of single photons for optical communication," Phys. Rev. Lett. **94**(15), 153901 (2005).
10. J. A. Anguita, M. A. Neifeld, and B. V. Vasic, "Turbulence-induced channel crosstalk in an orbital angular momentum-multiplexed free-space optical link," Appl. Opt. **47**(13), 2414–2429 (2008).

#148481 - $15.00 USD Received 1 Jun 2011; revised 27 Jun 2011; accepted 29 Jun 2011; published 11 Jul 2011

11. J. Leach, J. Courtial, K. Skeldon, S. M. Barnett, S. Franke-Arnold, and M. J. Padgett, "Interferometric methods to measure orbital and spin, or the total angular momentum of a single photon," Phys. Rev. Lett. **92**(1), 013601 (2004).
12. G. Gibson, J. Courtial, M. Padgett, M. Vasnetsov, V. Pas'ko, S. Barnett, and S. Franke-Arnold, "Free-space information transfer using light beams carrying orbital angular momentum," Opt. Express **12**(22), 5448–5456 (2004).
13. M. T. Gruneisen, W. A. Miller, R. C. Dymale, and A. M. Sweiti, "Holographic generation of complex fields with spatial light modulators: application to quantum key distribution," Appl. Opt. **47**(4), A32–A42 (2008).
14. M. P. C. Fossorier, "Quasi-cyclic low-density parity-check codes from circulant permutation matrices," IEEE Trans. Inf. Theory **50**(8), 1788–1793 (2004).
15. S. Lin and D. J. Costello, *Error Control Coding: Fundamentals and Applications* (Prentice Hall, 2004).
16. I. B. Djordjevic, M. Arabaci, and L. Minkov, "Next generation FEC for high-capacity communication in optical transport networks," J. Lightwave Technol. **27**(16), 3518–3530 (2009).
17. J. Chen, A. Dholakia, E. Eleftheriou, M. Fossorier, and X.-Y. Hu, "Reduced-complexity decoding of LDPC codes," IEEE Trans. Commun. **53**(8), 1288–1299 (2005).
18. I. B. Djordjevic and M. Arabaci, "LDPC-coded orbital angular momentum (OAM) modulation for free-space optical communication," Opt. Express **18**(24), 24722–24728 (2010).
19. J. D. Jackson, *Classical Electrodynamics* (Wiley, 1975).
20. I. B. Djordjevic, M. Arabaci, L. Xu, and T. Wang, "Generalized OFDM (GOFDM) for ultra-high-speed optical transmission," Opt. Express **19**(7), 6969–6979 (2011).
21. H. G. Batshon and I. B. Djordjevic, "Beyond 240 Gb/s per wavelength optical transmission using coded hybrid subcarrier/amplitude/ phase/polarization modulation," IEEE Photon. Technol. Lett. **22**(5), 299–301 (2010).
22. H. G. Batshon, I. B. Djordjevic, L. Xu, and T. Wang, "Multidimensional LDPC-coded modulation for beyond 400 Gb/s per wavelength transmission," IEEE Photon. Technol. Lett. **21**(16), 1139–1141 (2009).
23. I. B. Djordjevic and H. G. Batshon, "Generalized hybrid subcarrier/amplitude/phase/polarization LDPC-coded modulation based FSO Networking," in *Proceedings of IEEE 12th International Conference on Transparent Optical Networks (ICTON 2010)* (IEEE, 2010), paper Th.B3.4.
24. W. Shieh and I. B. Djordjevic, *OFDM for Optical Communications* (Elsevier/Academic Press, 2009).
25. S. M. Alamouti, "A simple transmit diversity technique for wireless communications," IEEE J. Sel. Areas Comm. **16**(8), 1451–1458 (1998).
26. A. Goldsmith, *Wireless Communications* (Cambridge University Press, 2005).
27. D. Tse and P. Viswanath, *Fundamentals of Wireless Communication* (Cambridge University Press, 2005).
28. T. M. Duman and A. Ghrayeb, *Coding for MIMO Communication Systems* (Wiley, 2007).
29. I. B. Djordjevic, L. Xu, and T. Wang, "PMD compensation in multilevel coded-modulation schemes with coherent detection using BLAST algorithm and iterative polarization cancellation," Opt. Express **16**(19), 14845–14852 (2008).
30. J. G. Proakis, *Digital Communication* (McGraw Hill, 2001).
31. I. B. Djordjevic and G. T. Djordjevic, "On the communication over strong atmospheric turbulence channels by adaptive modulation and coding," Opt. Express **17**(20), 18250–18262 (2009).
32. I. B. Djordjevic, "Adaptive modulation and coding for communication over the atmospheric turbulence channels," in *Proceedings of IEEE Photonics Society Summer Topicals* (IEEE, 2009), paper TuD3.3.
33. M. Arabaci, I. B. Djordjevic, R. Saunders, and R. M. Marcoccia, "Polarization-multiplexed rate-adaptive non-binary-quasi-cyclic-LDPC-coded multilevel modulation with coherent detection for optical transport networks," Opt. Express **18**(3), 1820–1832 (2010).

1. Introduction

Power-efficient modulation schemes, such as pulse-position modulation (PPM), are widely adopted in current deep-space optical communications [1–6]. The very large bandwidth of these links (compared to RF links) has made the low spectral efficiency of PPM less of a concern. However, in order to achieve multi-gigabit transmission (projected for 2020) for the use in interplanetary communications [5], the use of large number of time slots in PPM is needed, which imposes stringent requirements on system design and implementation. On the other hand, we have shown recently [7,8] that through the use of orbital angular momentum (OAM) modulation we can satisfy high-bandwidth demands of future interplanetary communications, while keeping the system cost and power consumption reasonably low. The OAM is associated with azimuthal phase of the complex electric field. Because OAM eigenstates are orthogonal, in principle, arbitrary number of bits per single photon can be transmitted. The ability to generate/analyze states with different OAMs, by using interferometric or holographic methods [9–13] allows the realization of deep-space/near-Earth optical communication systems with ultra-high photon efficiencies expressed in terms of number of bits per photon. The OAM modulation and multiplexing can, therefore, be used, in combination with other degrees of freedom, to solve the high-bandwidth requirements of future deep-space and near-Earth optical communications. By increasing the number of OAM

#148481 - $15.00 USD Received 1 Jun 2011; revised 27 Jun 2011; accepted 29 Jun 2011; published 11 Jul 2011

states we can increase the aggregate data rate of the system, while enabling reliable transmission at these higher speeds by using low-density parity-check (LDPC) codes [14–17]. Dramatic increase in photon efficiency through OAM modulation and multiplexing will provide revolutionary capabilities for future deep-space/near-Earth applications. The main challenge for OAM deep-space communication represents the link between a spacecraft probe and the Earth station because in the presence of atmospheric turbulence the orthogonality between OAM states is no longer preserved.

In this paper, we will show that in combination with LDPC codes, OAM-based modulation schemes can operate even under strong atmospheric turbulence regime. The following multi-gigabit enabling approaches for deep-space and near-Earth optical communications based on OAM are described: (i) OAM multiplexing (Sec. 2); (ii) *N*-dimensional OAM modulation (Sec. 2); and (iii) orthogonal OAM division multiplexing (Sec. 3), similar to OFDM [24]. We will also describe different approaches to deal with atmospheric turbulence induced OAM crosstalk including: (1) equalization; (2) OAM-time coding, which is analogous to the space-time coding; and (3) adaptive modulation and coding (AMC).

Notice that our previous paper on OAM modulation [18] deals with terrestrial FSO communications, and it employs volume holograms to perform OAM modulation/demodulation, while in this paper instead we use multimode fiber (MMF) to perform OAM modulation/demodulation. Moreover, Ref. [18] does not discuss at all neither orthogonal OAM division multiplexing nor compensation of OAM crosstalk effects introduced by atmospheric turbulence. Further, we provide detailed description of OAM demodulator and iterative demapper/decoder. Finally, we describe both direct detection and coherent detection OAM demodulators.

The paper is organized as follows. In Section 2, we describe the concepts of OAM multiplexing and modulation. We also describe an *N*-dimensional OAM-based coded modulation scheme suitable for deep-space and near-Earth applications. The OAM division multiplexing is described in Section 3. Different methods to re-establish the orthogonality of OAM modes, after transmission over atmospheric turbulence channels, are described in Section 4. We evaluate the suitability of OAM-based coded-modulation schemes for deep-space/near-Earth applications in Section 5. Section 6 is devoted to concluding remarks.

2. Deep-space and near-Earth optical Communications based on LDPC-coded OAM modulation

In this section, we describe how to simultaneously increase the photon and spectral efficiencies based on *N*-dimensional OAM coded modulation. The angular momentum, $\boldsymbol{L}$, of the classical electromagnetic field can be written as [19]

$$\boldsymbol{L} = \frac{1}{4\pi c}\int_V \boldsymbol{E}\times\boldsymbol{A}dV + \frac{1}{4\pi c}\int_V \sum\nolimits_{k=x,y,z} E_k\left(\boldsymbol{r}\times\nabla\right)A_k dV, \qquad (1)$$

where $\boldsymbol{E}$ is the electric field intensity, $\boldsymbol{A}$ is the vector potential associated with magnetic field intensity $\boldsymbol{H}$ by $\boldsymbol{H}=\nabla\times\boldsymbol{A}$ and electric field intensity by $\boldsymbol{E} = -c^{-1}\partial\boldsymbol{A}/\partial t$, and c is the speed of light. The second term in (1) is identified with the OAM because of the presence of the angular momentum operator $\boldsymbol{r}\times\nabla$ term. Among various optical beams that can carry OAM, Laguerre-Gauss (LG) vortex beams can easily be implemented. For example, a field distribution of LG beam traveling along z-direction can be expressed in cylindrical coordinates (r,ϕ,z) (r denotes the radial distance from propagation axis, ϕ denotes the azimuthal angle and z denotes the propagation distance) as follows [10]:

$$u_{l,p}\left(r,\phi,z\right) = \sqrt{\frac{2p!}{\pi\left(p+|l|\right)!}}\frac{1}{w(z)}\left[\frac{r\sqrt{2}}{w(z)}\right]^{|l|} L_p^l\left(\frac{2r^2}{w^2(z)}\right) e^{-\frac{r^2}{w^2(z)}} e^{-\frac{jkr^2 z}{2\left(z^2+z_R^2\right)}} e^{j\left(2p+|l|+1\right)\tan^{-1}\frac{z}{z_R}} e^{-jl\phi}, \qquad (2)$$

#148481 - $15.00 USD Received 1 Jun 2011; revised 27 Jun 2011; accepted 29 Jun 2011; published 11 Jul 2011

where $w(z) = w_0[1 + (z/z_R)]^{1/2}$ with w_0 being the zero-order Gaussian radius at the waist, $z_R = \pi w_0^2 / \lambda$ is the Rayleigh range (with λ being the wavelength), $k = 2\pi/\lambda$ is the propagation constant, and $L^l_p(\cdot)$ is the associated Laguerre polynomial, with p and l representing the radial and azimuthal mode numbers, respectively. It can be seen from (2) that lth mode of LG beam has the azimuthal angular dependence of the form $\exp(-jl\phi)$, and consequently, l is also called the azimuthal mode number (index). For $l = 0$, field $u(r,\phi,z)$ becomes a zero-order Gaussian beam, that is the TEM_{00} mode. For $p = 0$, $L^l_p(\cdot) = 1$ for all ls, so that the intensity of a LG mode is a ring of radius proportional to $(|l|)^{1/2}$, as illustrated in Fig. 1(a). It can be shown [10] that for fixed p, the following principle of othogonality is satisfied:

$$\left(u_{m,p}, u_{n,p}\right) = \int u^*_{m,p}\left(r,\phi,z\right) u_{n,p}\left(r,\phi,z\right) r dr d\phi = \begin{cases} \int \left|u_{m,p}\right|^2 r dr d\phi, & n = m \\ 0, & n \neq m \end{cases} \quad (3)$$

Clearly, different OAM states for fixed p are mutually orthogonal and as such they can be used as basis functions for *OAM modulation*. The number of OAM states to be used depends on atmospheric turbulence strength. For $N = 2L + 1$, the corresponding OAM states can be indexed by l where l takes values in the set $\{-L,-L + 1,\ldots,-1,0,1,\ldots,L\}$. By increasing the number of dimensions (i.e., the number of OAM eigenstates), we can increase the aggregate data rate of the system.

The transmitter and receiver block diagrams for OAM modulation are shown in Fig. 1. Previously, we studied the use of volume holograms based multidimensional *terrestrial* FSO communication [18]. The terrestrial FSO system described in [18] employs the volume holograms to perform OAM multiplexing/de-multiplexing. Instead of using the set of holograms to impose different OAM states, here we use mode multiplexer/demultiplexer based on multimode fibers as shown in Fig. 1(b)/(c). During mode multiplexing, a continuous wave laser diode signal is split into N branches by using a power splitter (such as 1:N star coupler) to feed N Mach-Zehnder modulators (MZMs), each corresponding to one of the N OAM modes. The mode demultiplexer can be implemented by propagating the multimode signal in opposite direction, as shown in Fig. 1(c). The jth input to the jth MZM, $1 \le j \le N$, corresponds to the jth coordinate of the signal to be modulated (see Fig. 1b). The output of mode multiplexer is expanded by telescope and transmitted towards remote destination. The OAM multiplexing is obtained by summing up N independent streams per each OAM state into a single optical beam. Clearly, when OAM transmitter and receiver are implemented as shown in Fig. 1(b,c) we are not able to distinguish between OAM modes with azimuthal mode numbers of the same magnitude but of opposite sign. Nevertheless, distinguishable modes $l = 0,1,\ldots,L$ (for fixed p) are still orthogonal. The mode detector shown in Fig. 1(e), instead of being implemented based on Fig. 1(c) it can be implemented based on integrated ring-shaped detector with N-different p.i.n. regions to capture different l-modes, as illustrated in Fig. 1(a) for $p = 0$. Such a mode detector will have N outputs that correspond to N-projections along OAM modes. After this generic description of OAM based deep-space/near-Earth optical communication systems, we provide more details of OAM transmitter and receiver.

The K different bit streams coming from different information sources are encoded using (n,k_m) $(m = 1,\ldots,K)$ LDPC codes, as shown in the Fig. 1(d). The outputs of the encoders are interleaved by the $K \times n$ block interleaver. The block interleaver accepts bits from the encoders row-wise and outputs bits column-wise to the mapper, which accepts K bits at each time instance i. The mapper determines the corresponding M^N-ary signal constellation point by

$$s_i = C_N \sum\nolimits_{j=1}^{N} \varphi_{i,j} \Phi_j;\ i = 1,2,\cdots,M^N \quad (4)$$

where M is the number of amplitude levels per OAM state and C_N is the normalization constant. The set $\{\Phi_1, \Phi_2,\ldots,\Phi_N\}$ represents a set of N orthogonal OAM basis functions, while with $\varphi_{i,j}$ we denoted OAM modulation coordinates of ith constellation point. The signals are

#148481 - $15.00 USD Received 1 Jun 2011; revised 27 Jun 2011; accepted 29 Jun 2011; published 11 Jul 2011

then modulated, mode multiplexed and sent over the deep-space or near-Earth optical channel (see Fig. 1).

The number OAM modes N to be used is determined by the desired final rate and current channel conditions. The simplest OAM-based coded modulation scheme with direct detection can be described by the following set of constellation points for N = 3 and M = 2 {(0,0,0),

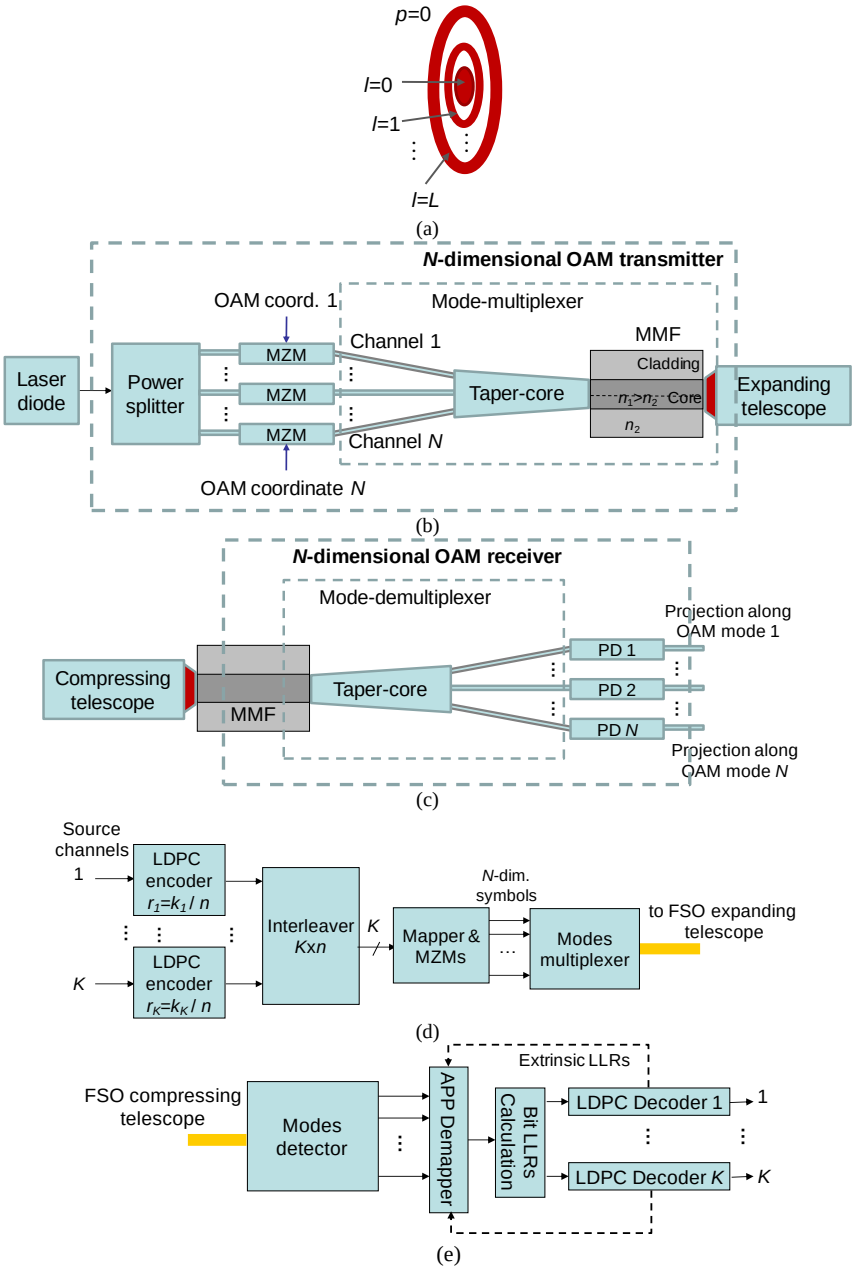

Fig. 1. Multidimensional LDPC-coded OAM modulation scheme: (a) intensity spatial distribution for p = 0, (b) MMF-based mode-multiplexer and N-dimensional transmitter configurations, (c) MMF-based N-dimensional OAM receiver, (d) overall transmitter architecture and (e) overall receiver architecture. MZM: Mach-Zehnder modulator, MMF: multimode fiber, PD: photodetector, APP: *a posteriori* probability, LLRs: log-likelihood ratios.

#148481 - $15.00 USD Received 1 Jun 2011; revised 27 Jun 2011; accepted 29 Jun 2011; published 11 Jul 2011

(0,0,1), (0,1,0), (0,1,1), (1,0,0), (1,0,1), (1,1,0), (1,1,1)}. The *N*-dimensional signal constellation can be obtained as the *N*-dimensional Cartesian product of a one-dimensional signal constellation originating from non-negative pulse-amplitude modulation (PAM). At the receiver side (see Fig. 1(d)), after OAM demodulation (or mode demultiplexing) and photodetection, the outputs of the *N* branches of the demodulator are sampled at the symbol rate, and the corresponding samples, after analog-to-digital conversion, are forwarded to the *a posteriori* probability (APP) demapper. The orthogonality among OAM modes in realistic deep-space and near-Earth optical communication systems can be re-established by various MIMO and equalization techniques, as discussed in Section 4. The APP demapper provides the bit LLRs required for iterative LDPC decoding (see Fig. 1e). The *l*th branch in Fig. 1(f) represents the projection along *l*th OAM state (coordinate). Let

$$\boldsymbol{S}_i = \left[S_i^{(-L)}\ S_i^{(-L+1)} \cdots S_i^{(-1)}\ S_i^{(0)}\ S_i^{(1)} \cdots S_i^{(L)} \right]^T$$

denote the transmitted signal constellation point for system shown in Fig. 1(a), $\boldsymbol{R}_i$ denote the received constellation point, and $\boldsymbol{S}_0$ denote the reference constellation point. The superscript (*l*) (*l* = -*L*,…,-1,0,1…,*L*) is used to denote the *l*th OAM coordinate. When the deep-space/near-Earth optical communication system is based on *N*-dimensional transmitter and receiver shown in Fig. 1(c,d), then the corresponding signal constellation point is defined as $\boldsymbol{S}_i = \left[S_i^{(0)}\ S_i^{(1)} \cdots S_i^{(N-1)} \right]^T$. Let $P(\boldsymbol{R}_i|\boldsymbol{S}_i)$ denote the conditional probabilities that are estimated by collection of OAM crosstalk histograms, obtained by propagating sufficiently long training sequence over the deep-space/near-Earth optical channel, while $P(\boldsymbol{S})$ denotes *a priori* probability of symbol $\boldsymbol{S}$. The symbol log-likelihood ratios (LLRs) can be calculated by

$$\lambda(\mathrm{S}_i) = \log\left[\frac{P(\mathrm{S}_i|\mathrm{R}_i)}{P(\mathrm{S}_0|\mathrm{R}_i)} \right], \tag{5}$$

where $P(\mathrm{S}_i|\mathrm{R}_i)$ is determined by Bayes' rule as

$$P(\boldsymbol{S}_i|\mathrm{R}_i) = \frac{P(\mathrm{R}_i|\mathrm{S}_i')P(\mathrm{S}_i)}{\sum_{\mathrm{S}'} P(\mathrm{R}_i|\mathrm{S}_i')P(\mathrm{S}_i')}. \tag{6}$$

By substituting Eq. (6) into Eq. (5) we obtain

$$\lambda(\mathrm{S}_i) = \log\left[\frac{P(\mathrm{R}_i|\mathrm{S}_i)P(\mathrm{S}_i)}{P(\mathrm{R}_i|\mathrm{S}_0)P(\mathrm{S}_0)} \right] = \log\left[\frac{P(\mathrm{R}_i|\mathrm{S}_i)}{P(\mathrm{R}_i|\mathrm{S}_0)} \right] + \log\left[\frac{P(\mathrm{S}_i)}{P(\mathrm{S}_0)} \right] = \log\left[\frac{P(\mathrm{R}_i|\mathrm{S}_i)}{P(\mathrm{R}_i|\mathrm{S}_0)} \right] + \lambda_a(\mathrm{S}_i), \tag{7}$$

where $\lambda_a(\mathrm{S}_i) = \log\left[P(\mathrm{S}_i)/P(\mathrm{S}_0) \right]$. Let us denote by c_j the *j*th bit in the observed symbol $\boldsymbol{S}$ binary representation $\boldsymbol{c} = (c_0, c_1, \ldots, c_{b-1})$ (*b* is the number of bits needed to represent the symbol $\boldsymbol{S}$). The prior symbol LLRs for the next iteration are determined by

$$\lambda_a(\boldsymbol{S}) = \log\frac{P(\boldsymbol{S}_0)}{P(\boldsymbol{S}_i)} = \log\frac{\prod_{j=0}^{b-1} P(c_j = 0)}{\prod_{j=0}^{b-1} P(c_j)} = \sum_{j=0}^{b-1} \log\frac{P(c_j = 0)}{P(c_j)}. \tag{8}$$

Because

#148481 - $15.00 USD Received 1 Jun 2011; revised 27 Jun 2011; accepted 29 Jun 2011; published 11 Jul 2011

$$\log\frac{P(c_j=0)}{P(c_j)}=\begin{cases}0, & c_j=0\\ L(c_j), & c_j=1\end{cases}=c_jL(c_j), \tag{9}$$

where $L(c_j) = \log[P(c_j = 0)/P(c_j = 1)]$, the prior symbol LLRs become

$$\lambda_a(\boldsymbol{s})=\sum_{j=1}^{b}c_jL(c_j). \tag{10}$$

Finally, the prior symbol estimate can be obtained from

$$\lambda_a(\hat{\boldsymbol{s}})=\sum_{j=1}^{b}c_jL_{D,e}(c_j), \tag{11}$$

where

$$L_{D,e}(\hat{c}_j)=L\left(c_j^{(\mathrm{out})}\right)-L\left(c_j^{(\mathrm{in})}\right). \tag{12}$$

In Eq. (12), we use $L(c^{(\mathrm{in})}_j)$ [$L(c^{(\mathrm{out})}_j)$] to denote the LDPC decoder input (output). The bit LLRs $L(c_j)$ are determined from symbol LLRs by

$$L(\hat{c}_j)=\log\frac{\sum_{\boldsymbol{c}:c_j=0}\exp[\lambda(\boldsymbol{S})]\exp\left(\sum_{\boldsymbol{c}:c_k=0,k\neq j}L_a(c_k)\right)}{\sum_{\boldsymbol{c}:c_j=1}\exp[\lambda(\boldsymbol{S})]\exp\left(\sum_{\boldsymbol{c}:c_k=0,k\neq j}L_a(c_k)\right)}. \tag{13}$$

Therefore, the jth bit reliability is calculated as the logarithm of the ratio of a probability that $c_j = 0$ and probability that $c_j = 1$. In the nominator, we perform the summation over all symbols $\boldsymbol{S}$ having 0 at the observed position j, while in the denominator over all symbols $\boldsymbol{S}$ having 1 at the same position j. With $L_a(c_k)$ we denoted the prior (extrinsic) information determined from the APP demapper. The inner summation in (13) is performed over all bits of symbol $\boldsymbol{S}$, selected in the outer summation, for which $c_k = 0$, $k \neq j$. The bit LLRs are forwarded to LDPC decoders, which provide extrinsic bit LLRs for demapper according to (12), and are used as inputs to (11) as the prior information.

Notice that deep-space/near-Earth optical communication systems shown in Fig. 1 are based on direct detection. When coherent detection is used, the corresponding modulator can be: (i) one-dimensional MZM biased at null point (see Fig. 1(b)), (ii) two-dimensional modulator based on I/Q modulator (see Fig. 2(a)) and (iii) four-dimensional (see Fig. 2(b)). When I/Q modulator is used, in addition to N OAM orthogonal modes, we employ the in-phase (I) and quadrature (Q) components so that the corresponding space is 2N-dimensional. On the other hand, when four-dimensional modulator is used, with two coordinates being I- and Q-coordinates in x-polarization and two coordinates being I- and Q-coordinates in y polarization, the corresponding space is 4N-dimensional. The 4N-dimensional scheme allows even 4N-bits to be transmitted per single symbol, which represents an energy-efficient communication scheme. However, the complexity of such receiver might be too high even for near-Earth applications. The one-dimensional coherent detection scheme seems to be a good compromise between optical link energy-efficiency and receiver complexity. In Fig. 2(c), we show the receiver configuration with coherent detection that assumes that one-dimensional MZMs are used. One laser is used to detect all coordinates, whose output is used as an input to 1:N power splitter. The output of balanced detector n (n = 0,1,…,N-1) provides the projection along OAM state n. This coherent detection receiver scheme; composed of mode-demultiplexer, balanced coherent detectors, power splitter and local laser; can be integrated on a single chip using hybrid opto-electronic integrated circuit (OEIC) technology.

Notice that different orthogonal basis functions can be used instead of orthogonal OAM eigenstates (e.g., [20], [21–23]). For example, the orthogonal subcarriers can be used as the

#148481 - $15.00 USD Received 1 Jun 2011; revised 27 Jun 2011; accepted 29 Jun 2011; published 11 Jul 2011

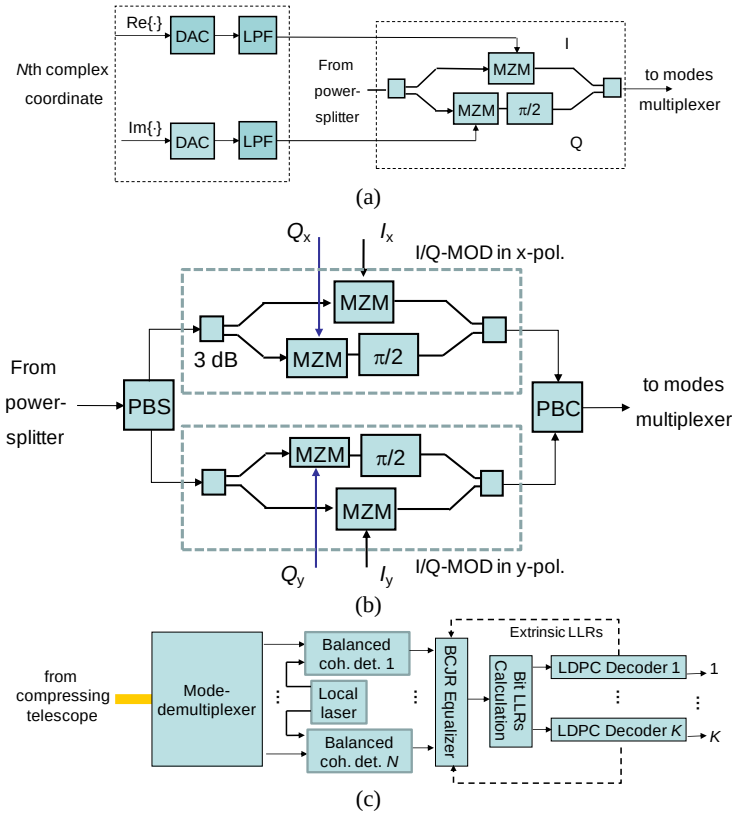

Fig. 2. Coherent detection based OAM modulation: (a) two-dimensional modulator, (b) four-dimensional modulator and (c) coherent receiver architecture (corresponding to one-dimensional modulators).

basis functions for multidimensional signaling, which was the subject of Ref. [20]. However, the subcarrier-based multidimensional signaling cannot be used to simultaneously improve SNR sensitivity and spectral efficiency. For example, if we are concerned with SNR sensitivity we can use the orthogonal subcarriers as basis functions in multidimensional signaling to increase the Euclidean distance between signal constellation points, while keeping the total signal bandwidth the same. In proposed scheme, however, we can simultaneously improve the SNR sensitivity and spectral efficiency. Namely, by increasing the number of OAM eigenstates, used for basis functions, we can dramatically increase the aggregated data rate, while keeping the symbol rate fixed, as the increase of the number of OAM modes does not lead to bandwidth expansion. In order to achieve multi-gigabit transmission, which is projected for 2020, for the use in interplanetary communications [5], the use of better spectral efficient schemes, such as proposed one, is needed. The current deep-space optical communications are based on PPM, and in order to achieve the multi-Gb/s data rate, predicted by Hemmati in [5], a huge number of time-slots will be needed in PPM, which introduces too stringent requirements from implementation point of view.

3. Orthogonal OAM division multiplexing

The transmitter and receiver configurations for orthogonal OAM division multiplexing are shown in Fig. 3(a), and (b), respectively. It has certain similarities with OFDM [24]. The transmitter configuration up to the mapper is very similar to that shown in Fig. 1(e). The mapper accepts K bits at time instance i from the ($K \times n$) interleaver column-wise and determines the corresponding M-ary ($M = 2^K$) signal constellation point ($\phi_{I,i}$, $\phi_{Q,i}$) assuming a

#148481 - $15.00 USD Received 1 Jun 2011; revised 27 Jun 2011; accepted 29 Jun 2011; published 11 Jul 2011

two-dimensional (2D) constellation such as *M*-ary PSK or *M*-ary QAM. The coordinates correspond to in-phase (I) and quadrature (Q) components of *M*-ary 2D constellation. The 2D constellation points, after serial-to-parallel (S/P) conversion, are used as the inputs to I/Q modulators of OAM transmitters shown in Fig. 3(a). On the receiver side, upon OAM demultiplexing and detection as shown in Fig. 3(b), the soft estimates of symbols $\tilde{s}_k$ carried by *k*th OAM state are forwarded to the APP demapper, which determines the symbol LLRs. The soft symbol estimates in the *k*th OAM state $\tilde{s}_k$ are obtained by using one of the OAM-crosstalk compensation techniques described in next section. The bit LLRs needed for LDPC decoders are calculated in the bit LLR calculation block in similar fashion to that described in Section 2.

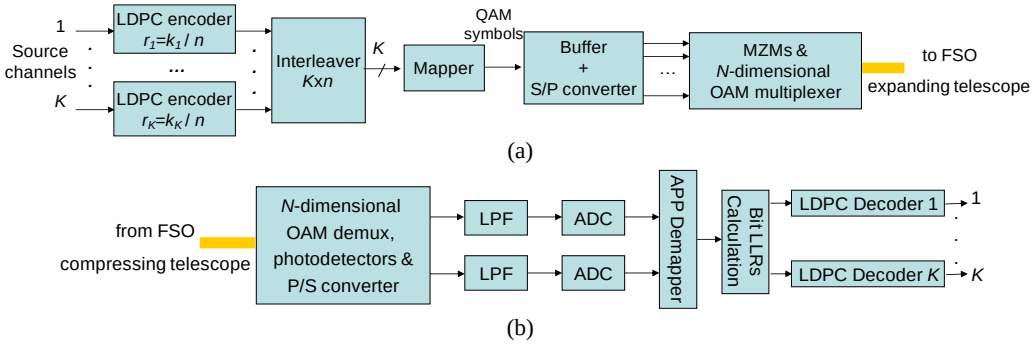

Fig. 3. Deep-space optical communication by orthogonal OAM division multiplexing: (a) transmitter and (b) receiver configurations.

4. Compensation of OAM crosstalk introduced by atmospheric turbulence

In this section, we describe several approaches to compensate for atmospheric turbulence effects.

OAM Channel Model

Atmospheric turbulence is caused by variations in the refractive index of the transmission medium due to inhomogeneities in temperature and pressure caused by solar heating and wind. The optical turbulent channel has been intensively studied, and various models have been proposed to describe turbulence-induced performance degradation [6]. The OAM-based FSO channel model with coherent detection can be described as follows:

$$\boldsymbol{y} = \boldsymbol{H}\boldsymbol{x} + \boldsymbol{w}, \quad \boldsymbol{H} = \begin{bmatrix} h_{11} & h_{12} & \dots & h_{1,N} \\ h_{21} & h_{22} & \dots & h_{2,N,} \\ \dots & \dots & \dots & \dots \\ h_{N,1} & h_{N,2} & \dots & h_{N,N} \end{bmatrix}, \tag{14}$$

where $\boldsymbol{x} = [x_1\ x_2\ \dots\ x_N]^T$ is transmitted vector with *i*th complex number component being the in-phase/quadrature (I/Q) signal constellation point transmitted using *i*th OAM state; $\boldsymbol{y} = [y_1\ y_2\ \dots\ y_N]^T$ is the received vector; $\boldsymbol{w} = [w_1\ w_2\ \dots\ w_N]^T$ is the vector of noise samples; and $\boldsymbol{H}$ represents the channel matrix with rank($\boldsymbol{H}$) = *N* that corresponds to the number of OAM states not experiencing fading (due to atmospheric turbulence). The channel matrix coefficients can be determined by using a training sequence. The OAM FSO channel model (14) is similar to a wireless communication MIMO model [25–29] and, therefore, different techniques used in spatial interference cancellation are directly applicable here. Below we describe equalization, OAM-time coding, and adaptive modulation and coding. Other methods suitable to deal with atmospheric turbulence induced crosstalk among OAM states include: OAM diversity; linear

#148481 - $15.00 USD Received 1 Jun 2011; revised 27 Jun 2011; accepted 29 Jun 2011; published 11 Jul 2011

interfaces: zero-forcing interface and minimum mean-square error (MMSE) interface; nonlinear interfaces: vertical and diagonal BLAST [29], iterative atmospheric turbulence cancellation; parallel decomposition of OAM-MIMO by singular value decomposition (SVD) of the channel matrix; and OAM-beam forming.

OAM crosstalk compensation by equalization

The scalar representation of Eq. (14),

$$y_i = \sum_{j=1}^{N} h_{i,j} x_j + w_i; \quad i = 1, 2, \cdots, N \tag{15}$$

indicates that *i*th OAM detector output can be represented as a finite impulse response (FIR) filter. That is, the channel model (15) is similar to an intersymbol interference (ISI) model so that various channel equalization techniques [26–30] can be used to compensate for OAM crosstalk including a feed-forward equalizer (FFE), decision-feedback equalizer (DFE), maximum-likelihood sequence detector (MLSD), and a turbo equalizer.

OAM-time coding

If we allow the signal designs to be extended over multiple OAM states and over multiple symbol times, we can refer to these designs as the OAM-time codes, in analogy to the space-time codes used in wireless communications [25–29]. Most space-time codes designed for wireless communications are straightforwardly applicable here, but they are most probably not optimal. Under the assumption that the FSO channel is quasi-static for the duration of N_s symbols, which is true for multi-gigabit transmission, the OAM FSO channel inputs and outputs are matrices, with dimensions corresponding to space-coordinate (the number of OAM modes) and time-coordinate (the number of symbol intervals). This can be modeled by

$$\boldsymbol{Y} = \boldsymbol{H}\boldsymbol{X} + \boldsymbol{W}, \tag{16}$$

where

$$\begin{gathered} \boldsymbol{Y} = \left[\boldsymbol{y}_1, \boldsymbol{y}_2, ..., \boldsymbol{y}_{N_s} \right] = (Y_{ij})_{N \times N_s}, \boldsymbol{X} = \left[\boldsymbol{x}_1, \boldsymbol{x}_2, ..., \boldsymbol{x}_{N_s} \right] = (X_{ij})_{N \times N_s} \\ \boldsymbol{W} = \left[\boldsymbol{w}_1, \boldsymbol{w}_2, ..., \boldsymbol{w}_{N_s} \right] = (W_{ij})_{N \times N_s} \end{gathered} \tag{17}$$

and where N is the number of OAM modes. Let us observe an OAM-time code in which the receiver has the knowledge of the channel matrix $\boldsymbol{H}$. Under maximum-likelihood (ML) detection, the optimum transmit matrix is obtained by the following minimization:

$$\hat{\boldsymbol{X}} = \arg \min_{\boldsymbol{X} \in X^{N \times N_s}} \sum_{i=1}^{N_s} \left\| \boldsymbol{y}_i - \boldsymbol{H}\boldsymbol{x}_i \right\|^2, \tag{18}$$

where the minimization is performed over all possible OAM-time input matrices.

Adaptive modulation and coding (AMC)

There are many parameters that can be varied at the transmitter side to accommodate FSO channel conditions, including data rate, power, coding rate, and combinations of different adaptation parameters. In several of recent papers (e.g., [31–33]), we have studied various adaptive modulation and coding schemes suitable for dealing with atmospheric turbulence for different multilevel modulation schemes. This study can be extended to coded OAM modulation schemes.

5. Performance analysis

In Fig. 4, we show the BER performance of (girth-12, column-weight-3) LDPC(15120,7560)-coded N-dimensional (ND) OAM modulation versus PPM. On horizontal axis we use average

#148481 - $15.00 USD Received 1 Jun 2011; revised 27 Jun 2011; accepted 29 Jun 2011; published 11 Jul 2011

number of photons per dimension (in dB-scale) so that ND-OAM and PPM can be compared. The results of simulations shown in Figs. 4-6 are obtained for Poisson deep-space optical channel model for the average number of background photons of 0.1. We assume that residual crosstalk on a given OAM mode is given by n_x = 0.1. From Fig. 4 it is clear that as we increase the number of dimensions, the improvement of ND-OAM over PPM is larger. The improvement (measured at BER of 10^{-6}) ranges from 0.67 dB for N = 2 to 2.81 dB for N = 8. Moreover, the spectral efficiency S_E of ND-OAM is

$$\frac{S_{E,\text{ND-OAM}}}{S_{E,\text{PPM}}} = \frac{\log_2 2^N / (1/T_s)}{\log_2 M / (M/T_s)} = \frac{N}{\log_2 M / M} \tag{19}$$

times better than that of PPM. In (19), with T_s we denoted the signaling interval (reciprocal of a symbol rate). For the same number of dimensions (M = N), the spectral efficiency of ND-OAM is $N^2/\log_2 N$ times better. For example, for M = N = 8, the spectral efficiency of ND-OAM is 21.334 times better.

In Figs. 5-6, we evaluate performance of LDPC-coded ND-OAM in the presence of atmospheric turbulence, under medium (Fig. 5) and strong (Fig. 6) turbulence regimes. (For definition of Rytov standard deviation σ_R see [6].) For N = 8, the degradation in performance ranges from 2.02 dB in medium turbulence regime to 2.87 dB in strong turbulence regime (at BER of 10^{-6}).

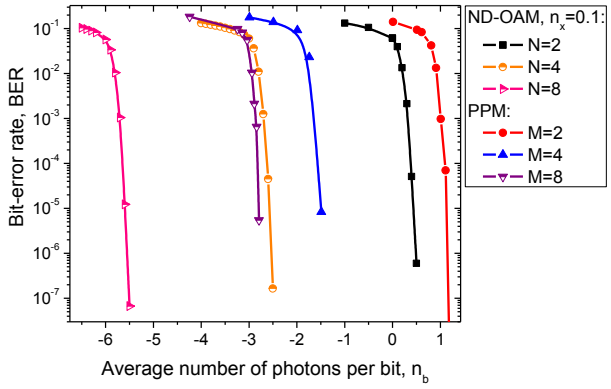

Fig. 4. LDPC(15120,7560)-coded ND-OAM modulation versus PPM.

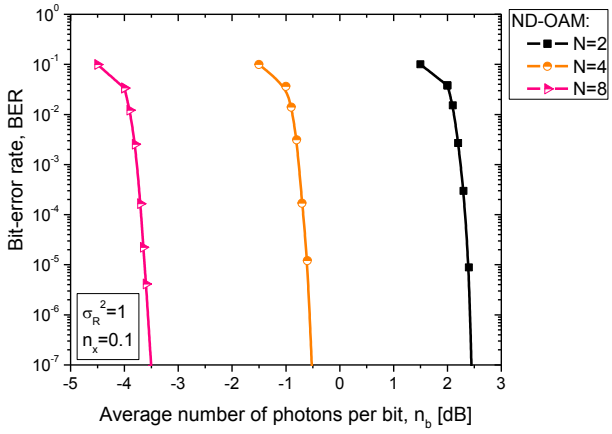

Fig. 5. LDPC(15120,7560)-coded ND-OAM modulation in medium turbulence regime (σ_R = 1).

#148481 - $15.00 USD Received 1 Jun 2011; revised 27 Jun 2011; accepted 29 Jun 2011; published 11 Jul 2011

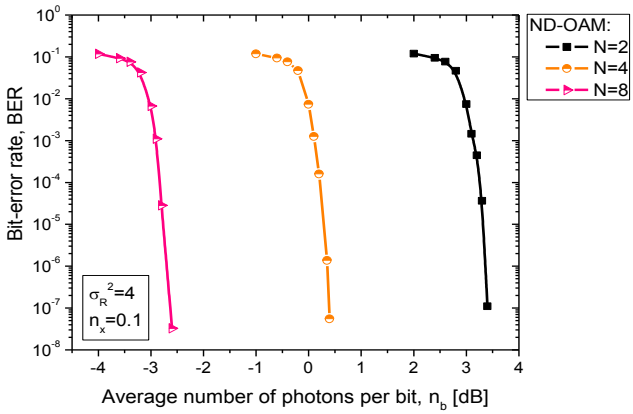

Fig. 6. LDPC(15120,7560)-coded ND-OAM modulation in strong turbulence regime (σ_R = 2).

In Fig. 7, we evaluate (girth-8, column-weight-4) LDPC(4320,3242)-coded ND-OAM scheme for use in near-Earth applications. Both direct and coherent detection schemes are evaluated. In simulations, we assume that OAM crosstalk distribution follows the Gaussian distribution (the same assumption was used in [10]), which motives the use of signal-to-noise-and-crosstalk ratio (SCNR) instead of signal-to-noise ratio (SNR). Direct detection schemes can operate properly in weak turbulence regime, while in strong turbulence regime they exhibit error floor phenomena (not shown in figure) and as such must be combined with repetition MIMO schemes. On the other hand, the coherent detection schemes with M = 2 and $N \geq 2$ can operate even in strong turbulence regime for reasonable high SCNRs, as shown in Fig. 7.

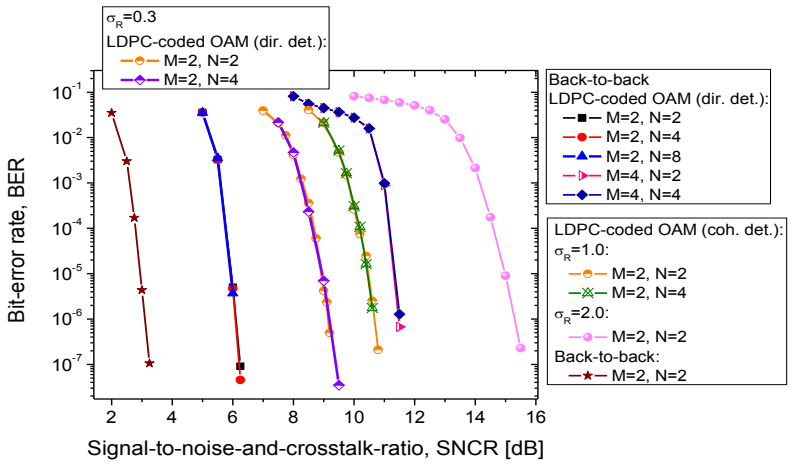

Fig. 7. BER performance of LDPC(4320,3242)-coded OAM modulation based FSO systems in weak (σ_R = 0.3), medium (σ_R = 1) and strong (σ_R = 2) turbulence regimes.

6. Concluding remarks

In this paper, we studied the use of OAM as an additional degree of freedom for modulation and multiplexing in deep-space and near-Earth applications. The following multi-gigabit enabling approaches for deep-space communication based on OAM have been described: OAM multiplexing, N-dimensional OAM modulation, and orthogonal OAM division multiplexing. We demonstrate by Monte Carlo simulations, over the atmospheric turbulence channels, that proposed schemes can operate under strong atmospheric turbulence and provide dramatic improvement in throughput. We have shown that the improvement of ND-OAM

#148481 - $15.00 USD Received 1 Jun 2011; revised 27 Jun 2011; accepted 29 Jun 2011; published 11 Jul 2011

over PPM, for the same number of dimensions, (measured at BER of 10^{-6}) ranges from 0.67dB for $N = 2$ to 2.81 dB for $N = 8$. Moreover, the spectral efficiency, for the same number of dimensions, of ND-OAM is $N^2/\log_2 N$ times better. The proposed OAM-based schemes, therefore, represent the excellent candidates for next generation deep-space and near-Earth optical communications. In addition to next generation deep-space/near-Earth optical communication enabling technologies, we have described different approaches to deal with atmospheric turbulence induced OAM crosstalk including equalization, OAM-time coding, and adaptive modulation and coding.

Notice there is a significant effort to improve the result from [2] in terms coming closer to the channel capacity limits. Some researchers are trying to improve this result even for a fraction of dB. With the proposed scheme, however, we are able to outperform LDPC-coded PPM for even 2.81 dB for $N = 8$, and at the same time improve spectral efficiency 21 times (also for $N = 8$), indicating that the proposed scheme is a promising candidate for next generation deep-space and near-Earth optical communications.

Some other applications of interest of OAM-based systems described in this paper include: providing ultra-high-speed Internet connection, increasing data rate and reducing system cost and deployment time in access networks, enabling ground-to-satellite/satellite-to-ground FSO communications at high-speed, enabling ultrahigh-speed intersatellite communications, and possibly enabling aircraft-to-satellite/ satellite-to-aircraft high-data-rate communications.

Acknowledgments

This work was supported in part by the National Science Foundation (NSF) under Grants CCF-0952711 and ECCS-0725405.

#148481 - $15.00 USD Received 1 Jun 2011; revised 27 Jun 2011; accepted 29 Jun 2011; published 11 Jul 2011